Sulfate affinity controls phosphate sorption and the proto-transformation of schwertmannite

Karel As [a,*], Stefan Peiffer [a], Peter Onyisi Uhuegbue [a,b], Prachi Joshi [c], Andreas Kappler [c,d], Bouchra Marouane [a], Kerstin Hockmann [a,e]

[a] University of Bayreuth, Bayreuth Center for Ecology and Environmental Research (BayCEER), Department of Hydrology, Universitätstraße 30-GEO II, 95440 Bayreuth, Germany
[b] Leibniz Centre for Agricultural Landscape Research, ZALF, Eberswalder Str. 84, 15374 Müncheberg, Germany
[c] University of Tübingen, Geomicrobiology, Department of Geosciences, Schnarrenbergstraße 94-96, 72076 Tübingen, Germany
[d] University of Tübingen, Cluster of Excellence EXC 2124: Controlling Microbes to Fight Infections, Auf der Morgenstelle 28, 72076 Tübingen, Germany
[e] University of Bayreuth, Bayreuth Center for Ecology and Environmental Research (BayCEER), Experimental Biogeochemistry, Dr.-Hans-Frisch-Straße 1-3, 95448 Bayreuth, Germany

ARTICLE INFO

ABSTRACT

Schwertmannite is a metastable sulfate-rich ferric iron Fe(III) (oxyhydr)oxide and a common mineral in acid mine drainage sites and acid sulfate soils. Schwertmannite is also used as a sorbent in various industrial applications, including phosphate removal in water treatment and environmental remediation. Phosphate sorption to schwertmannite, however, is complex and likely involves ligand exchange for inner- and outer-spherically co-ordinated sulfate groups, both on the surface and in the tunnel structure of the mineral. Here, we investigated phosphate sorption, concomitant sulfate release and their impact on the structure of schwertmannite as a function of pH and phosphate concentration. Kinetic and equilibrium batch experiments with synthetic schwertmannite were carried out at pH 3, 6, and 8, and the solid-phase was analyzed using a combination of microscopic, spectroscopic, and X-ray diffraction techniques. We found a strong correlation between phosphate sorption and sulfate release, with both following a two-step sorption model. The kinetics of phosphate sorption and sulfate release were faster at higher pH levels. Maximum phosphate sorption was found at pH 6 (1.7 mmol PO_4^{3-} g^{-1}), which decreased to 1.5 and 1.2 mmol PO_4^{3-} g^{-1} at pH 3 and 8, respectively. Fourier transform infrared spectroscopy revealed a shift from inner- to outer-spherical coordination of sulfate with increasing pH. ^{57}Fe-Mössbauer analyses of schwertmannite demonstrated an initial transformation of schwertmannite at neutral to alkaline pH, characterized by a rise in a partially ordered sextet area. This change was interpreted as an increase in crystallinity resulting from the transition from Fe-SO$_4$ to Fe—O domains. The emerging phase differed from the original schwertmannite, but did not represent a complete change to a new crystalline phase, thus indicating a proto-transformation of schwertmannite. This pH-induced proto-transformation was inhibited in the presence of phosphate. We concluded that the phosphate sorption rate and maximum as well as the proto-transformation of schwertmannite were strongly affected by the mineral's affinity for sulfate. Sorption to schwertmannite should primarily be regarded as a competitive exchange reaction between the sorbing oxyanion and the bound sulfate. As a result, the highest phosphate sorption occurred at circumneutral pH, in stark contrast to non-sulfate-containing Fe(III) (oxyhydr)oxides, where phosphate sorption is highest at acidic pH. Our findings are important for a fundamental understanding of the sorption properties of schwertmannite in phosphate-rich environments as they point towards the central role of sulfate coordination for phosphate immobilization.

1. Introduction

Schwertmannite (Fe$_8$O$_8$(OH)$_{8-2x}$(SO$_4$)$_x$, where x ranges from 1 to 1.75) is a sulfate-rich ferric iron Fe(III) (oxyhydr)oxide characterized by low crystallinity and high surface area (Bigham et al., 1994; Bigham et al., 1990). It is a common mineral in environments with low pH values (pH 3–5), such as acid mine drainage sites and acid sulfate soils (Regenspurg et al., 2004; Fitzpatrick et al., 2017a). In these environments, schwertmannite plays a key role in controlling water quality by acting as a high-affinity, high-capacity sorbent for toxic and polluting oxyanions, such as molybdate, chromate, arsenate and phosphate (Schoepfer and Burton, 2021; Burton et al., 2021). These properties also make schwertmannite a promising sorbent material in environmental remediation (Simon and Burghard, 2016; Marouane et al., 2021).

The structure of schwertmannite has not been fully resolved due the mineral's metastability, small particle size, and variable elemental composition (Paikaray et al., 2011; Liu et al., 2015; Schoepfer and Burton, 2021). Certain studies have even proposed that schwertmannite may exhibit a polyphasic nature (French et al., 2012), where nano-sized crystalline features are embedded within an amorphous matrix. Nevertheless, schwertmannite is most frequently described as having an akageneite-like structure with iron octahedra forming a tunnel framework, which is stabilized by sulfate groups in the tunnel cavities ("tunnel sulfate") (Bigham et al., 1990). Additional sulfate groups are distributed on the mineral's surface ("surface sulfate") (Bigham et al., 1990; Jönsson et al., 2005), but tunnel sulfate comprises the majority (50–65%) of the total sulfate content (Bigham et al., 1990; Rose and Ghazi, 1997; Paikaray and Peiffer, 2010; Wang et al., 2015). Independent of its location, sulfate can occur as both inner- and outer-sphere complexes (Boily et al., 2010; Fernandez-Martinez et al., 2010; Wang et al., 2015). The release of sulfate results in the collapse of the tunnel structure and thus leads to the mineralogical transformation of schwertmannite, ultimately yielding goethite as the end product (Regenspurg et al., 2004; Knorr and Blodau, 2007).

Schwertmannite can sorb up to a quarter of its weight in phosphate (PO$_4^{3-}$, a term used here to encompass protonated and deprotonated phosphate species) and thus contributes to the low phosphorus availability in acid sulfate systems (Bai et al., 2021; Eskandarpour et al., 2006; Schoepfer et al., 2017). Only few studies have investigated schwertmannite interactions with phosphate, but most of them suggest that phosphate sorption involves exchange with sulfate and hydroxyl groups (Fukushi et al., 2004; Schoepfer and Burton, 2021). Ligand-exchange with sulfate appears to serve as the primary sorption mechanism, occurring both in the tunnels and on the mineral's surface (Burton et al., 2009; Antelo et al., 2012). Inner- and outer-sphere sulfate complexes participate in the exchange, but oxyanions that form inner-sphere complexes appear to preferably exchange for inner-sphere coordinated sulfate groups (Wang et al., 2021). Substitution of schwertmannite's sulfate groups by the larger phosphate ions may also induce a structural distortion which, in turn, can impact the sorption properties of schwertmannite (Regenspurg and Peiffer, 2005; Fan et al., 2023). In contrast, Schoepfer et al. (2019, 2021) have shown that high levels of phosphate can also stabilize schwertmannite against conversion to more crystalline minerals such as goethite by decreasing the mineral's solubility. However, these studies were conducted under anoxic conditions where Fe(II) facilitated the transformation of schwertmannite, possibly overlooking initial structural changes. Importantly, phosphate may exert contrasting effects on schwertmannite stability, whereby it can both promote and inhibit schwertmannite transformation, depending on the environmental conditions and temporal scope of investigation.

In natural environments, schwertmannite is formed at low pH and sorption studies have thus far primarily focused on acidic conditions (Fukushi et al., 2004; Khamphila et al., 2017; Schoepfer et al., 2017; Fan et al., 2023). As a result, phosphate sorption at circumneutral pH remains largely unexplored, despite its significance for human-impacted and engineered systems. For instance, in cultivated acid sulfate soils,

where schwertmannite and phosphate co-occur (Fitzpatrick et al., 2017a), liming is a common practice, resulting in near-neutral pH values of the topsoil (Sarangi et al., 2022). Furthermore, pH can fluctuate strongly in these soils due to the impact of alternating flood-drought conditions (Fitzpatrick et al., 2017b). Schwertmannite has also been proposed as a sorbent material for the remediation of wastewater and phosphate-laden eutrophic surface waters with near-neutral pH (Simon and Burghard, 2016; Marouane et al., 2021). Consequently, schwertmannite may be exposed to both high-pH environments and substantial phosphate loadings.

Understanding schwertmannite's environmental persistence and its interactions with phosphate across diverse pH conditions is important for a mechanistic understanding of its role as a phosphate sink in nutrient-rich environments. In particular, changes in sulfate coordination, its impact on phosphate sorption and the consequences for the mineralogical characteristics of schwertmannite remain unexplored. This study therefore investigated phosphate sorption and concomitant sulfate release at pH 3, 6, and 8 using equilibrium and kinetic sorption experiments with synthetic schwertmannite. To explore shifts in mineralogy influenced by pH or phosphate sorption, the solid-phase was analyzed using a combination of microscopic, spectroscopic, and X-ray diffraction techniques.

2. Methods

2.1. Schwertmannite synthesis

Schwertmannite was synthesized based on the step-wise oxidation method by Liu et al. (2015), which is an adaptation of the fast peroxide method (Regenspurg et al., 2004). Using 30 L-reactors, a large-scale synthesis was performed by dissolving 889.6 g of FeSO$_4 \bullet 7$ H$_2$O in 20 L deionized water to create a 160 mM Fe(II) solution. While stirring, a total of 240 mL of a 32% H$_2$O$_2$-solution was added in 60 mL steps at 0, 8, 24 and 36 h. After Fe(II) oxidation was completed, precipitates were allowed to settle, overlying water was removed, and precipitates were washed using deionized water. These washing cycles were repeated until the conductivity of the solution was <150 μS cm^{-1}. The precipitates were dried for 72 h at 40 °C. Determination of total iron and sulphur contents of the solids was performed by dissolving 0.2 g of the product in a 40 mL solution of 6 M HCl for 48 h on a shaker (Winland et al., 1991). Iron and sulphur concentrations in the digests were determined by inductively coupled plasma-optical emission (ICP-OES, Perkin Elmer OPTIMA 3200 XL). The S:Fe ratio was used to determine the stoichiometry of schwertmannite as per its general composition (Fe$_8$O$_8$(OH)$_{8-2x}$(SO$_4$)$_x \bullet$ nH$_2$O, where $1 < x < 1.75$).

2.2. Sulfate release as a function of pH

Suspension of schwertmannite in an electrolyte solution typically results in an immediate exchange of hydroxyl ions with sulfate from schwertmannite. We therefore investigated the relationship between sulfate release and consumption of hydroxyl ions during a 24-h pre-equilibration period prior to start of the sorption experiments (Section 2.3). To this end, 10 g schwertmannite was added to 1 L of a 10 mM NaCl solution at pH of 3,6 or 8. The pH was kept constant during pre-equilibration by addition of a 1 M NaOH solution using a pH-stat device (Metrohm 716 DMS Titrino). The device also recorded the volume of the added base, allowing to determine the ratio of consumed hydroxide ions and released sulfate. Samples were taken at 0, 0.25, 0.5, 1, 2, 3, 5, and 24 h and the suspensions were filtered through 0.45 μm polyamide (PA) filters (Macherey-Nagel Gmbh). The filtrates were stored at −20 °C until further analysis.

2.3. Sorption isotherm analysis

Sorption isotherms were obtained by performing batch experiments

in 50 mL vials containing a 10 g L^{-1} suspension of schwertmannite in 40 mM NaCl at pH 3, 6, and 8 (in duplicates). Solutions were buffered using 40 mM PIPPS (pKa = 3.73) for pH 3, 40 mM MES (pKa = 6.15) for pH 6-, and 40 mM PIPES (pKa = 6.76) for pH 8. These buffers were chosen as they are recognized for their minimal interaction with mineral surfaces (Yu et al., 1997). This was verified by comparing sulfate release in systems with buffers to those using a pH-stat device (Supporting Information SI 1).

Suspending schwertmannite in solution leads to the exchange of hydroxide ions with rapidly exchangeable sulfate, causing solution acidification and potential pH deviations. To address this, schwertmannite was pre-equilibrated without phosphate for 24 h, allowing pH to stabilize before phosphate was added. Three hours before this equilibration period ended, the pH was measured and, if required, re-adjusted by dropwise addition of a 2 M NaOH solution. Once pre-equilibration was complete, the sorption reaction was initiated by adding the appropriate amount of a 1 M NaH_2PO_4 stock solution, resulting in a final volume of 40 mL. Initial PO_4^{3-}-concentrations of 0, 1, 2, 4, 6, 8, 10, 12, 14, 16, 18 and 20 mM were added to the reaction vials, yielding PO_4^{3-} : schwertmannite ratios from 0.1 to 2 mmol PO_4^{3-} per gram schwertmannite. The sorption reaction was allowed to equilibrate for 24 h on an overhead shaker. Subsequently, the solid and liquid phases were separated by centrifugation (5000 rpm, 10 min). The liquid phase was decanted and filtered through 0.45 μm PA filters and the solids were freeze-dried and ground for further analysis. The amount of sorbed phosphate was calculated from the difference between the initial and equilibrium aqueous phosphate concentrations. Fitting of the data occurred with the Freundlich equation (Eq. (1)) using the non-linear fitting package *nlstools* in R (Baty et al., 2015):

$$Q_{PO4} = K_f * C_{eq}^{\frac{1}{n}} \qquad (1)$$

where Q_{PO4} is the sorbed PO_4^{3-} on schwertmannite in mmol PO_4^{3-} g^{-1}, K_f is the partition coefficient, n is a measure of the affinity of schwertmannite for PO_4^{3-}, and C_{eq} is the PO_4^{3-} concentration at the end of equilibration in mmol L^{-1}. Note that all sorption experiments were performed under atmospheric conditions. Thermodynamic modeling in PHREEQC was used to confirm that formation of dissolved carbonate by dissolution of carbon dioxide did not interfere with surface processes. (SI 2). We also used PHREEQC 3.0 (Appelo and Postma, 2013) to model the ligand exchange reaction between phosphate and sulfate groups.

2.4. Kinetic sorption analysis

Kinetic sorption experiments were performed in duplicate using 1-L reaction vessels at pH 3, 6, and 8. The same buffer and electrolyte concentrations as in the batch sorption experiments were employed and the same methods for pre-equilibration and pH adjustment were followed. Phosphate was added at initial phosphate concentrations of 0, 1, 10, and 20 mM, resulting in a zero- (0 mmol PO_4^{3-} g^{-1}), low- (0.1 mmol PO_4^{3-} g^{-1}), medium- (1 mmol PO_4^{3-} g^{-1}), and high-phosphate (2 mmol PO_4^{3-} g^{-1}) treatment, equivalent to molar P:Fe ratios of 0.01 to 0.2. The phosphate loadings were chosen based on the results from the sorption isotherms to achieve differing levels of surface site coverages and because they are representative of the molar ratio between Fe(III) and associated phosphorus in oxic surface sediments (0.1–0.3) (Kraal et al., 2022; Kraal et al., 2020; Li et al., 2023). The suspension was constantly stirred during the experiment and 15 mL samples were taken with a syringe at reaction times of 0, 10, and 30 min as well as at 1, 2, 5, 24, 48, 168 and 226 h. The reaction was stopped by centrifugation (5000 rpm, 10 min), the aqueous phases were passed through 0.45 μm PA filters and the solids were freeze-dried and finely ground until further analysis.

2.5. Solid phase analyses

2.5.1. Scanning electron microscopy

The micromorphology of the solids before and after reaction with phosphate were examined by scanning electron microscopy (SEM). To this end, the ground and freeze-dried samples were coated with a thin layer of platinum by a Cressington 208 HR sputter coater. Images were recorded by secondary electron detectors on a Zeiss ULTRA PLUS microscope (Carl Zeiss Microscopy GmbH, Jena, Germany) operating at an acceleration voltage of 3 kV and a FEI Quanta 250 (Field Electron and Ion Company, Thermo Fisher Scientific, Hillsboro, USA) high-resolution field emission gun (FEG) scanning electron microscope at 10 kV.

2.5.2. BET-measurement

The specific surface area of freeze-dried and ground schwertmannite was determined by the Brunauer–Emmett–Teller (BET) method (Brunauer et al., 1938) on a Quantachrome Autosorb 1. 0.06 g of dried and ground schwertmannite was outgassed for 24 h in a nitrogen atmosphere at 90 °C. Following this, nitrogen gas (N_2) was allowed to physically adsorb onto the surface of schwertmannite at 77 K. The specific surface area was then calculated using the slope and intercept obtained by fitting the linear portion of a BET (Rouquerol et al., 2013). The detailed BET calculations are provided in SI 3.

2.5.3. Fourier Transformed Infrared (FTIR)

FTIR-spectra were collected with a Vektor 22 FTIR Spectrometer (Bruker). A portion (3 mg) of dried schwertmannite samples was mixed with anhydrous KBr (1:100 *w/w*, ground and pressed at 10 tons by a hydraulic press) to yield a solid pellet for analysis. A total of 32 scans was recorded in the wave number range of 5000 and 370 cm^{-1} at a 1 cm^{-1} resolution. The signal was averaged over these scans and a baseline correction was applied. Using the R package *nlstools* (Baty et al., 2015), Gaussian fitting was employed to determine the number and position of the principal phosphate and sulfate peaks. The averaged FTIR spectra were normalized and subsequently deconvoluted into a series of Gaussian curves as given by the parametric Gaussian equation (Eq. (2)):

$$f(x) = C * exp\left(\frac{(x - \mu)^2}{2\sigma}\right) \qquad (2)$$

where C denotes the maximum peak height, μ is the wave number around which the peak is centred, x is the wave number and σ is the broadness of the peak.

2.5.4. X-ray diffraction

Approximately 400 mg of the freeze-dried and ground powder was mounted into an XRD sample holder. Mineralogy was examined using X-ray diffraction (XRD) on randomly orientated powders with a Siemens D5000 X-Ray Diffractometer using a 40 mA and 40 kV Cobalt-K-alpha radiation (λ = 0.178897 nm). Scanning was performed from 20° to 80° 2θ with a step-size of 0.03° 2θ and a scanning time of 6 s per step. The resulting patterns were analyzed using the DIFFRAC-plu*s* evaluation software package (Bruker AXS, Karlsruhe, Germany) and the Crystallography Open Database (Gražulis et al., 2011).

2.5.5. Mössbauer spectroscopy

Changes in schwertmannite mineral structure after equilibration in the pH-buffered electrolyte in the presence and absence of phosphate were investigated by ^{57}Fe Mössbauer spectroscopy. Dried schwertmannite powders were loaded into plexiglass holders (area 1 cm^2), forming a thin disc. Holders were inserted into a closed-cycle exchange gas cryostat (Janis Research, USA) under a backflow of He to minimize exposure to air. Spectra were collected at 77 K and at 40 K using a
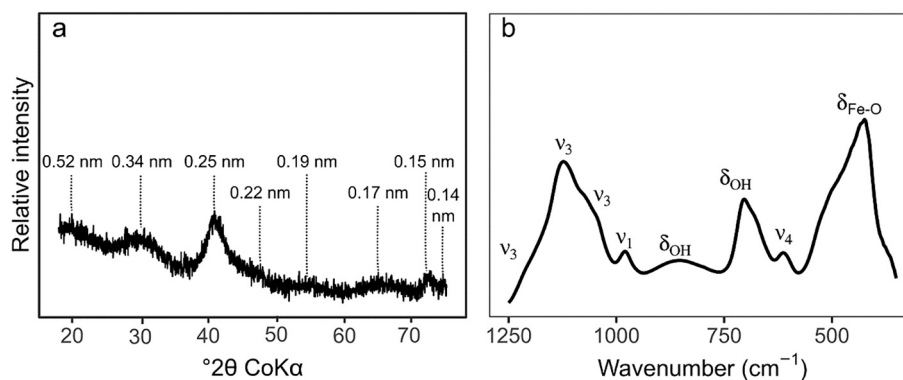
Fig. 1. (a) Characterization of the initial schwertmannite using X-ray diffractometry, with d-values (interplanar distances) annotated, and (b) FTIR spectrum of the initial schwertmannite.

constant acceleration drive system (WissEL, Germany) in transmission mode with a ^{57}Co/Rh source. All spectra were calibrated against a 7 μm thick α-^{57}Fe foil that was measured at room temperature. Analysis was conducted using the software *Recoil* (University of Ottawa) and the Voigt Based Fitting (VBF) routine (Lagarec and Rancourt, 1997). The half width at half maximum (HWHM) was constrained to 0.13 mm s^{-1} during fitting.

2.6. Aqueous phase analytical methods

Sulfate was measured photometrically using an acidified BaCl$_2$-solution containing 1 wt% of gelatine (Tabatabai, 1974). The samples' absorbance was determined after 60 min in a 3 mL cuvette at 420 nm.

Phosphate was measured photometrically based on the molybdate blue method (Murphy and Riley, 1958). The molybdate and sulfuric acid reagents were supplied by Merck ("o-phosphate Method," Spectroquant). Absorbance of the photometric complex was measured at 720 nm after a 10-min reaction time.

3. Results

3.1. Characterization of synthesized schwertmannite

The three-step hydrogen peroxide synthesis method (Liu et al., 2015) produced a mineral with a stoichiometry of Fe$_8$O$_8$(OH)$_{4.58}$(SO$_4^{2-}$)$_{1.71}$, corresponding to a sulfate content of 2.1 mmol SO$_4^{2-}$ g^{-1}. Scanning electron microscopy (SEM) revealed schwertmannites' distinctive pincushion morphology (Fig. SI2). Formation of schwertmannite was confirmed by structural analysis using XRD (Fig. 1a) and FTIR (Fig. 1b).

Analysis by X-ray diffraction showed eight broad Bragg diffraction peaks, typical of poorly crystalline schwertmannite (Bigham et al., 1990; Cornell and Schwertmann, 1996). The FTIR spectrum displayed the characteristic absorption bands for the S—O stretches (ν_3-peaks at 1170, 1120, 1050 cm^{-1} and ν_1 at 980 cm^{-1}) and bends (ν_4 at 610 cm^{-1}) (Boily et al., 2010). Peaks at 860 cm^{-1} and 712 cm^{-1} (δ_{OH}) correspond to OH-deformations typical for schwertmannite (Boily et al., 2010), and the peak at 425 cm^{-1} (δ_{Fe-O}) indicates an FeO stretching vibration (Bigham et al., 1990).

3.2. Aqueous phase results

3.2.1. Sulfate release during pre-equilibration

During pre-equilibration, sulfate release was rapid, and stable sulfate concentrations were reached after 5 to 10 h at all pH values (Fig. 2a). A more alkaline pH resulted in a faster initial sulfate release and a longer equilibration time. Initial sulfate release rates (determined from the first sampling points) increased approximately seven-fold over the investigated pH range, from 0.9 mmol SO$_4^{2-}$ g^{-1} h^{-1} at pH 3 to 6 mmol SO$_4^{2-}$ g^{-1} h^{-1} at pH 8. Also, the equilibrium sulfate concentration was substantially higher at a more alkaline pH. After 24 h, 11% of schwertmannite's initial sulfate was released at pH 3, which increased to 38% at pH 6 and 52% at pH 8, corresponding to 0.2, 0.9 and 1.3 mmol SO$_4^{2-}$ g^{-1}. No structural transformation occurred as evidenced by the FTIR and XRD (SI 5). Sulfate release was correlated with the addition of hydroxide ions at a constant 2 OH$^-$:1 SO$_4^{2-}$ ratio (Fig. 2b). Kinetic data for pH 3 and 6 were adequately fitted using a one-step pseudo-first order model, but for pH 8, a two-step model yielded statistically better results (SI 6).
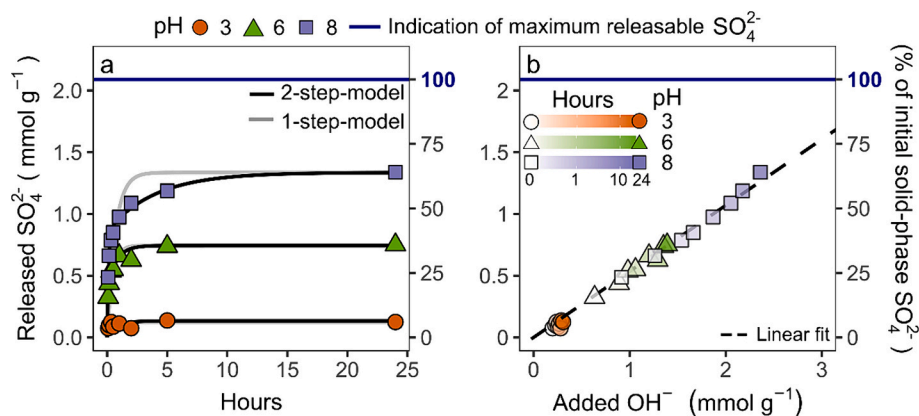
Fig. 2. Pre-equilibration of schwertmannite at pH 3, 6 and 8 in the absence of phosphate.
(a) Sulfate release during the 24-h pre-equilibration period. Kinetic models and fitting parameters are presented in SI 6. (b) Corresponding correlation between sulfate release and hydroxide addition The dashed line represents a linear fit with a slope of 0.49, suggesting that two hydroxyl groups replaced one sulfate group.
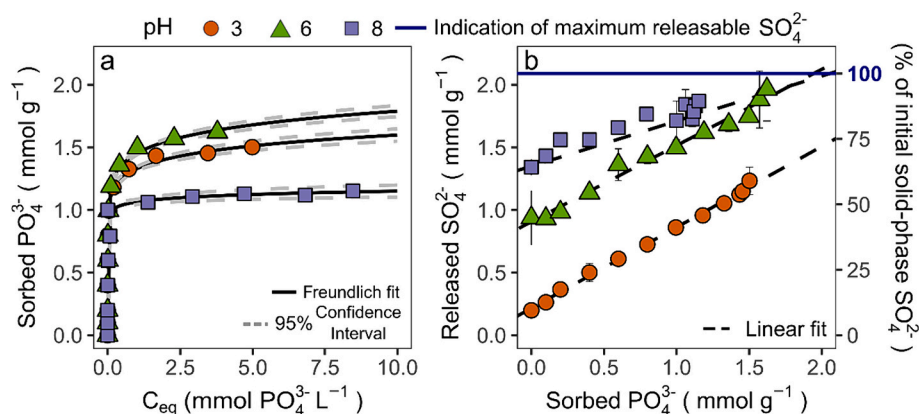
Fig. 3. (a) Phosphate sorption isotherms for schwertmannite at pH 3, 6 and 8.
(b) Correlation between released sulfate and sorbed phosphate. The blue horizontal line indicates the total sulfate amount in schwertmannite (i.e. the maximum releasable sulfate concentration). Freundlich fitting parameters are presented in SI 7. (For interpretation of the references to colour in this figure legend, the reader is referred to the web version of this article.)

3.2.2. Sorption isotherms

The influence of pH on phosphate sorption and concomitant sulfate release was explored by sorption isotherm experiments at pH 3, 6, and 8 (Fig. 3a). Sorption data were fitted using the Freundlich model. Schwertmannite had a high affinity for phosphate, and at all pH values, 100% of the added phosphate was sorbed up to a loading of 1 mmol PO_4^{3-} g^{-1} (Fig. 3a). The sorption maximum varied with pH and was highest at pH 6 (1.7 mmol PO_4^{3-} g^{-1}), while at pH 3 and pH 8, phosphate sorption reached only 1.5 and 1.2 mmol PO_4^{3-} g^{-1}, respectively, for the same added phosphate concentration (20 mmol L^{-1}). A plot of released sulfate against sorbed phosphate (Fig. 3b) revealed a linear relationship, suggesting a ligand-exchange mechanism. A 24-h pre-equilibration period without phosphate led to a release of 0.2, 0.8 and 1.2 SO_4^{2-} g^{-1} at pH 3, 6, and 8, accounting for 11%, 38%, and 52% of schwertmannite's initial sulfate. Conversely, sulfate release upon exchange with phosphate was highest at pH 6 and maximum phosphate loading, liberating 90% of schwertmannite's initial sulfate (1.9 mmol SO_4^{2-} g^{-1}).

For pH 8 and pH 3 at the highest phosphate loading, 80% (1.7 mmol SO_4^{2-} g^{-1}) and 60% (1.3 mmol SO_4^{2-} g^{-1}) of schwertmannite's initial sulfate was removed. The ligand exchange ratio (released sulfate:sorbed phosphate) slightly decreased with pH from 0.65 at pH 3 to 0.50 at pH 8.

3.2.3. Sorption kinetics

3.2.3.1. Phosphate sorption kinetics.
Sorption kinetics in the zero-, low-, medium- and high- phosphate treatments were fast, and equilibrium was achieved within 24 h at all pH values, except for the high phosphate treatment at pH 3 (Fig. 4a-c). The initial sorption rates (approximated based on the first measured time point at high phosphate loading) changed as a function of pH, amounting to 4.8 mmol PO_4^{3-} g^{-1} h^{-1} at pH 3, 6.8 mmol PO_4^{3-} g^{-1} h^{-1} at pH 6, and 6.1 mmol PO_4^{3-} g^{-1} h^{-1} at pH 8.

We used a one-step and a two-step model (Marouane et al., 2021) to fit kinetic sorption data, but the two-step model yielded significantly
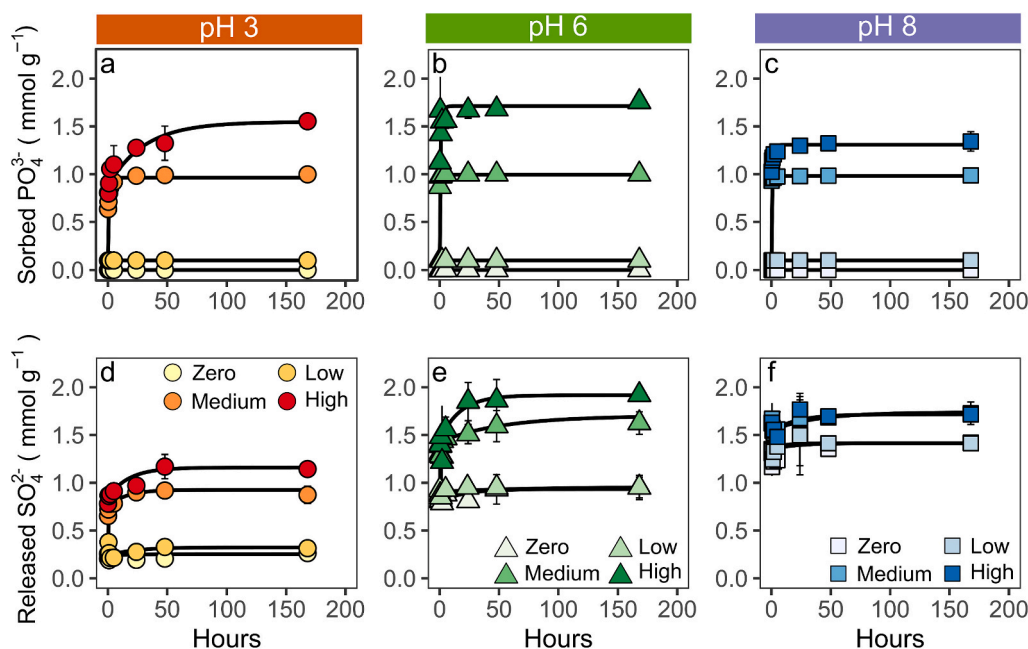

Fig. 4. Phosphate sorption to schwertmannite as a function of time at (a) pH 3, (b) 6, and (c) 8 in zero- (0 mmol PO_4^{3-} g^{-1}), low- (0.1 mmol PO_4^{3-} g^{-1}), medium- (1 mmol PO_4^{3-} g^{-1}) and high-PO_4^{3-} experiments (2 mmol PO_4^{3-} g^{-1}).
Concomitant sulfate release at (d) pH 3, (e) pH 6, and (f) pH 8. Fitting parameters of kinetic models and statistical analyses of the fits are provided in Tables 1, 2 and in the Supporting Information (SI 8–11).

Table 1

Fitting parameters for the kinetic sorption model of phosphate sorption to schwertmannite (Eq. (3)) during the experiments involving high phosphate concentrations (2 mmol PO_4^{3-} g^{-1}).

Sites per sorption pool (mmol PO_4^{3-} g^{-1})	pH 3	pH 6	pH 8
Fast-sorbed PO_4^{3-} ($Q_{PO4,fast-sorb}$)	0.7	1.1	1.0
Slowly sorbed PO_4^{3-} ($Q_{PO4,slow-sorb}$)	0.9	0.6	0.2
Total sorbed PO_4^{3-} ($Q_{PO4,tot-sorb}$)	1.5	1.7	1.3
Kinetic rate constants (h^{-1})			
Fast sorption ($k_{PO4,1}$)	>>[a]	>>[a]	>>[a]
Slow sorption ($k_{PO4,2}$)	0.03	0.68	0.63

[a] The fast sorption step occurred almost instantly, consistent with observations of phosphate sorption to goethite (Luengo et al., 2006).

better fits (SI 8). The two-step model posits the presence of both fast and slow sorption sites on schwertmannite. Quantification of the different sorption sites for the treatments was obtained from fitting the following model to the sorption data (Table 1):

$$Q_{PO4,tot} = Q_{PO4,fast-sorb} * \left(1 - e^{-kPO4,1*t}\right) + Q_{PO4,slow-sorb} * \left(1 - e^{-kPO4,2*t}\right) \qquad (3)$$

with $Q_{PO4,tot}$ quantifying the sorbed phosphate over time in mmol PO_4^{3-} g^{-1}, $Q_{PO4,fast-sorb}$ and $Q_{PO4,slow-sorb}$ denoting the amount of fast- and slowly sorbed phosphate in mmol PO_4^{3-} g^{-1}, t being time in h and $k_{PO4,1}$ and $k_{PO4,2}$ representing the fast and slow rate constants, expressed in units of h^{-1}.

Fitting was performed for all phosphate concentrations (SI 9). At low and medium phosphate levels, due to the rapid sorption kinetics and high sorption capacity, all phosphate was sorbed at the first measurement (10 min, low-phosphate) or within one hour (medium-phosphate treatments). The effects of pH were therefore most evident in the high-phosphate treatment. The fitted parameters for the high-phosphate experiment are shown in Table 1. The sorption process consisted of a fast step, which took <10 min to be completed ($k_{PO4,1}$, $Q_{PO4,fast-sorb}$), and a slow process ($k_{PO4,2}$, $Q_{PO4,slow-sorb}$), with pH affecting the kinetics and number of sites of both sorption processes. For the high phosphate treatment, the pool of the fast-sorbed phosphate sites ($Q_{PO4,fast-sorb}$) increased from 0.7 mmol PO_4^{3-} g^{-1} at pH 3 to ~1.0 at pH 6 and 8. As a proportion of the total phosphate added, this means that 76% of all phosphate sorption was fast for pH 8, which decreased to 65% and 44% at pH 6 and pH 3, respectively. Also, the rate constants of the slow process increased from 0.03 h^{-1} at pH 3 to 0.6–0.7 h^{-1} at pH 6 and 8. Consequently, attainment of sorption equilibrium at pH 3 in the high treatment took >100 h, while sorption equilibrium was reached within 24 h at pH 6 and pH 8.

3.2.3.2. Sulfate release kinetics. Sulfate release from schwertmannite was concurrently monitored with the sorption of phosphate (Fig. 4d-f). The released sulfate was a function of sorbed phosphate and pH. For

example, at the highest phosphate levels, sulfate release at pH 6 reached a maximum of 1.9 mmol SO_4^{2-} g^{-1}, followed by pH 8 (1.7 mmol SO_4^{2-} g^{-1}) and pH 3 (1.2 mmol SO_4^{2-} g^{-1}). Like the kinetic phosphate sorption models described above, we applied both a one-step and a two-step kinetic model to fit sulfate release. Consistent with our findings for phosphate sorption, the two-step model (Eq. (4)) generally resulted in better fits (SI 10). The model allowed us to categorize released sulfate into three operational pools: (i) sulfate released during pre-equilibration ($Q_{SO4,eq}$), (ii) fast-exchanged sulfate after phosphate addition ($Q_{SO4,fast-ex}$), and (iii) slowly exchanged sulfate after phosphate addition ($Q_{SO4,slow-ex}$). Quantification of these pools resulted from the model fitting process (Table 2), according to:

$$Q_{SO4,tot} = Q_{SO4,fast-ex} * \left(1 - e^{-kSO4,1*t}\right) + Q_{SO4,slow-ex} * \left(1 - e^{-kSO4,2*t}\right) + Q_{SO4,eq}$$

$$(4)$$

where $Q_{SO4,tot}$ represents the total released sulfate, $Q_{SO4,fast-ex}$ and $Q_{SO4,slow-ex}$ quantify the amounts of fast- and slowly exchanged sulfate, $Q_{SO4,eq}$ denotes sulfate released during the 24 h-pre-equilibration period (with all sulfate pools measured in mmol SO_4^{2-} g^{-1}), and $k_{SO4,1}$ and $k_{SO4,2}$ correspond to the fast and slow sulfate exchange rate constants, expressed in units of h^{-1}.

Fitting of sulfate release kinetics was performed for all phosphate loadings (SI 11), but as for phosphate, only the results from high loading are presented here. Like phosphate, the amount of sulfate that was rapidly released ($Q_{SO4,eq}$ and $Q_{SO4,fast-ex}$) increased with pH with 0.8 mmol SO_4^{2-} g^{-1} at pH 3, 1.3 mmol g^{-1} at pH 6, and 1.6 mmol g^{-1} at pH 8 (Table 2). The rate constants increased by a factor of ~5 when the pH increased ($k_{SO4,1}$ >> 67 h^{-1} for pH 6 and pH 8; $k_{SO4,1}$ = 14 h^{-1} for pH 3). Interestingly, the rate constant for the slowly exchanged sulfate pool was only marginally affected by pH ($k_{SO4,2}$ = 0.03–0.06). Overall, sulfate release was slower than the sorption of phosphate as revealed by the higher rate coefficients for both, the fast sorption ($k_{PO4,1}$) and slow sorption ($k_{PO4,2}$) processes.

3.3. Solid-phase analyses

3.3.1. Structural analysis: SEM

Potential changes in the morphology of schwertmannite before and after equilibration with phosphate were explored by SEM. Following a 24 h-equilibration period without phosphate (after pre-equilibration), no discernible morphological differences were observed compared to the initially synthesized schwertmannite (Fig. 5a-c, Fig. SI 3). Also, by XRD and FTIR no changes were observed (SI 12). The spherical shape and pin-cushion structure remained intact even though substantial amounts of schwertmannite's initial sulfate had been released at pH 6 (38% of total sulfate) and 8 (52%). Phosphate sorption led to additional sulfate loss, yet it did not result in substantial morphological alterations in the schwertmannite's appearance (Fig. 5d-f).

Table 2

Fitting parameters for the kinetic model describing sulfate release during sorption experiments involving high phosphate concentrations (Eq. (4)).

SO_4^{2-} release pools (mmol SO_4^{2-} g^{-1})	pH 3	pH 6	pH 8
SO_4^{2-} release during pre-equilibration ($Q_{SO4,eq}$)	0.2	0.9	1.4
Fast-exchanged SO_4^{2-} ($Q_{SO4,fast-ex}$)	0.6	0.4	0.2
Slowly-exchanged SO_4^{2-} ($Q_{SO4,slow-ex}$)	0.3	0.6	0.2
Total releasable SO_4^{2-} ($Q_{SO4,rel-tot}$)	1.2	1.9	1.7
Non-releasable ($SO_{4,non-rel}$)	0.9	0.2	0.4
Exchange ratio ($Q_{SO4,rel-tot}$: $Q_{PO4,tot-sorb}$)	0.8	1.2	1.5
Kinetic rate constants (h^{-1})			
Fast exchange ($k_{SO4,1}$)	14	>> 67[a]	>> 67[a]
Slow exchange ($k_{SO4,2}$)	0.06	0.03	0.05

[a] Sulfate release of the fast-exchange pool was practically instantaneous.
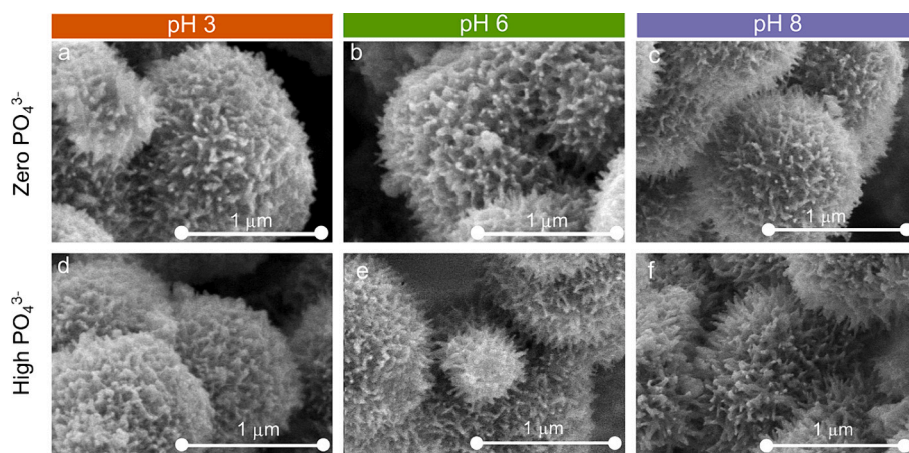
Fig. 5. SEM images of schwertmannite after 24 h of equilibration in the absence (a-c) and presence (d-f) of high levels of phosphate at pH 3, 6, and 8.

3.3.2. Structural analysis: FTIR

3.3.2.1. Effects of pH on sulfate coordination. FTIR spectra of schwertmannite were obtained after the 24-h pre-equilibration at pH 3, 6 and 8 (Fig. 6a). At pH 8, the peak area of the ν_3 sulfate vibration decreased, consistent with the greater sulfate release under alkaline conditions. In addition, the ν_3-peak position shifted to lower wave numbers as pH increased, moving from 1122 cm^{-1} at pH 3 to 1118 cm^{-1} at pH 6 and 1110 cm^{-1} at pH 8, thus suggesting alterations in sulfate coordination. Inner- and outer-sphere coordinated sulfate groups exhibit distinct FTIR spectra, but their peaks are not immediately discernible due to their coexistence in the schwertmannite structure, resulting in overlapping spectra. To assess the effect of pH on sulfate coordination, the spectra were deconvoluted using a method described by Jönsson et al. (2005).

In brief, a weighted pH 8-spectrum was subtracted from the pH 3- and pH 6-spectra and the process was also performed using the pH 3-spectrum for the pH 6- and pH 8-spectra (SI 13). The pH 3- and pH 8-spectra were considered as the end-members in coordination and through subtraction, spectral differences between the samples can be isolated. After Gaussian fitting, peaks at 1135 cm^{-1}, 1050 cm^{-1}, 1030

cm^{-1} and 985 cm^{-1} were identified in the pH 8 subtracted spectra at pH 3 and 6 (Fig. 6b). These peaks align with those observed for the inner-sphere sulfate FTIR spectrum (Wang et al., 2018) and were more intense for pH 3 than at pH 6. Conversely, when subtracting the pH 3-spectrum from the pH 6- and 8- spectra, distinct peaks at 1110 cm^{-1} and 1090 cm^{-1} emerged (Fig. 6c), which are characteristic for outer-sphere sulfate complexes (Wang et al., 2018). Outer-sphere sulfate contributions were largest at pH 8. Overall, spectral deconvolution demonstrated pH-dependent alterations in the proportion of differently coordinated sulfate complexes, with a higher pH increasing the amount of outer-sphere coordinated sulfate groups.

3.3.2.2. Phosphate coordination after sorption to schwertmannite. After sorption, phosphate had replaced a portion of the initially sorbed sulfate. FTIR was used to examine the coordination of sorbed phosphate. Phosphate and sulfate exhibit similar major vibrational peaks (SO$_4^{2-}$ at 1120 cm^{-1} and PO$_4^{3-}$ at 1080 cm^{-1}) due to their comparable molecular weight and structure (Coates, 2006). Especially at pH 3, substantial amounts of both phosphate (1.5 mmol PO$_4^{3-}$ g^{-1}) and sulfate (1.2 mmol SO$_4^{2-}$ g^{-1}) were present. The coexistence of phosphate in addition to
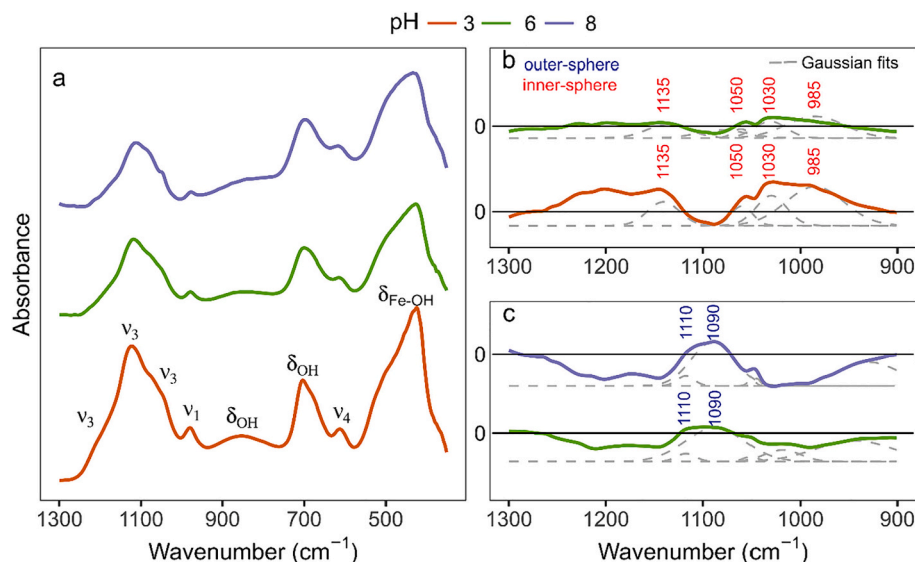
Fig. 6. FTIR analysis of sulfate coordination in schwertmannite.
(a) FTIR spectra after 24 h of equilibration at pH 3, 6, and 8 in the absence of phosphate. FTIR difference spectra resulting from subtracting (b) the pH 8-spectrum from the pH 3- and pH 6-spectra, or (c) the pH 3-spectrum from the pH 6- and pH 8-spectra. Grey dashed lines indicate Gaussian fits. Vibration peaks linked to outer-sphere sulfate complexes are marked in red, while those associated with inner-sphere complexes are indicated in blue. (For interpretation of the references to colour in this figure legend, the reader is referred to the web version of this article.)
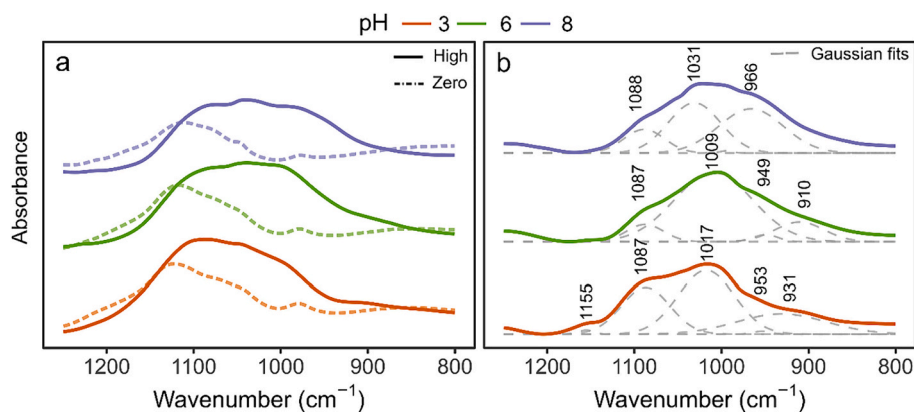
Fig. 7. FTIR analysis of phosphate coordination in schwertmannite.
(a) FTIR spectra after 24 h of equilibration with high levels of phosphate (solid lines) and in the absence of phosphate (dashed lines) at pH 3, 6, and 8. (b) Gaussian-fitted FTIR spectra of the high-phosphate treatments with the zero-treatment spectra subtracted.

non-exchanged sulfate resulted in the broadening of the ν_3-vibration band from 1200 to 1050 cm^{-1} to 1200–900 cm^{-1} (Fig. 7a). The spectrum was deconvoluted by subtracting the schwertmannite spectrum with zero loading from the phosphate-loaded spectra (Fig. 7a). This process removed the sulfate peaks, revealing the FTIR spectrum of the schwertmannite-bound phosphate (Fig. 7b).

Gaussian fitting was used to deconvolute the broad bands into distinct vibration peaks, which were found at 1087 cm^{-1}, 1010 to 1030 cm^{-1}, and 950 to 970 cm^{-1}. Position of the vibration peaks were similar to those previously ascribed to inner-sphere coordinated phosphate groups on ferrihydrite (1088 cm^{-1}, 1021 cm^{-1}, 952 cm^{-1}, Arai and Sparks, 2001). Generally, phosphate has been observed to form bidentate and monodentate surface complexes with iron oxides, which can be either protonated or deprotonated (Luengo et al., 2006; Elzinga and Sparks, 2007). The FTIR spectra showed slight variations as a function of pH, which may be due to the partial protonation of bidentate complexes under more acidic conditions (Elzinga and Sparks, 2007). Additionally, the formation of monodentate phosphate complexes, which are more favourable at lower pH levels, may also have contributed to these spectral changes (Arai and Sparks, 2001; Weng et al., 2020).

3.3.3. ^{57}Fe Mössbauer spectroscopy analyses

^{57}Fe Mössbauer spectroscopy was performed for both phosphate-sorbed (1 mmol PO$_4^{3-}$ g^{-1}) and phosphate-free schwertmannite samples at all pH conditions at a temperature of 77 K. The Mössbauer spectra were fitted with a broad collapsed sextet and one or two doublets, all indicative of Fe(III) (Fig. 8, Table 3). Such a mix of collapsed features and doublets is expected in schwertmannite at 77 K as the ordering temperature for schwertmannite has been reported to be between 120 and 60 K (Bigham et al., 1994; Eneroth and Bender, 2004; Cashion and Murad, 2012). In both sample spectra collected at pH 3 and the spectrum for phosphate-sorbed schwertmannite at pH 6, we observed asymmetrical features which we fit with two doublets. The asymmetry of schwertmannite spectra is consistent with previous studies (Bigham et al., 1994; Cashion and Murad, 2012). In samples where the proportion of the collapsed sextet was >90% of the total spectral area (pH 8 samples and phosphate-free pH 6 samples), the fitting was executed using only one doublet to prevent overfitting, which means that we tried to achieve an acceptable reduced χ^2 with the minimum number of fit components (Byrne and Kappler, 2022). The doublets used in the fitting had a centre shift (CS) between 0.3 and 0.6 mm s^{-1} and a quadrupole splitting (QS)

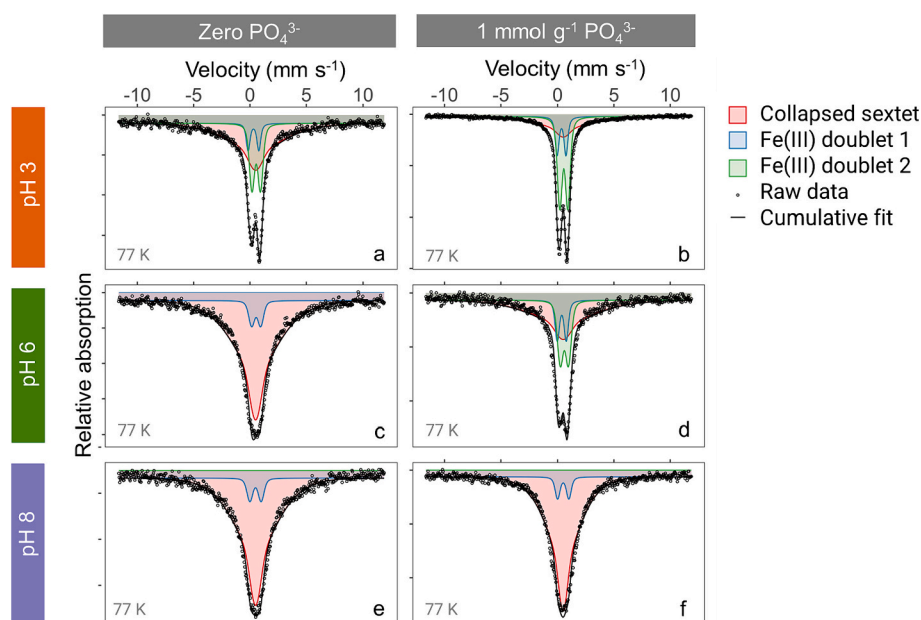**Fig. 8.** Comparison of ^{57}Fe Mössbauer spectra of schwertmannite reacted for 24 h at (a, b) pH 3, (c,d) pH 6, and (e,f) pH 8 in the absence and presence of phosphate. A uniform loading of 1 mmol PO$_4^{3-}$ g^{-1} was chosen for the phosphate treatments to facilitate better comparisons between spectra.

Table 3

Hyperfine parameters for ^{57}Mössbauer spectra collected at 77 K of phosphate-sorbed and phosphate-free samples at pH 3, 6, and 8.

Phosphate treatment	pH	Phase	CS[a] (mm s^{-1})	QS or ε[b] (mm s^{-1})	H[c] (T)	σ[d]	Relative area (%)	χ^2
		Fe(III) site 1	0.31	0.95			8.8	
		Fe(III) site 2	0.55	0.76			27.3	
Zero PO$_4^{3-}$	pH 3	Collapsed sextet	0.5	0	17.7	13.3	63.9	0.75
		Fe(III) site 1	0.35	0.79			17.1	
		Fe(III) site 2	0.55	0.72			47.7	
1 mmol PO$_4^{3-}$ g^{-1}	pH 3	Collapsed sextet	0.5	0	15.8	12	35.2	2.58
		Fe(III)	0.55	0.81			7.7	
Zero PO$_4^{3-}$	pH 6	Collapsed sextet	0.5	0	14.5	11	92.3	1.86
		Fe(III) site 1	0.37	0.8			13.8	
		Fe(III) site 2	0.6	0.73			27.7	
1 mmol PO$_4^{3-}$ g^{-1}	pH 6	Collapsed sextet	0.5	0	20	15.1	58.5	1.67
		Fe(III)	0.49	1			7.2	
Zero PO$_4^{3-}$	pH 8	Collapsed sextet	0.5	0	13.4	10.1	92.8	0.91
		Fe(III)	0.5	1			6.8	
1 mmol PO$_4^{3-}$ g^{-1}	pH 8	Collapsed sextet	0.49		10.5	8	93.2	1.7

[a] Center shift (relative to α-Fe^0).

[b] Quadrupole splitting (QS, paramagnetic) or quadrupole shift (ε, magnetic).

[c] Hyperfine magnetic field.

[d] Width of the collapsed sextet.

between 0.7- and 1-mm s^{-1} (Table 3).

The mix of a collapsed sextet and doublets in the spectrum represents the partial magnetic ordering of schwertmannite at 77 K (Bigham et al., 1994). To validate this interpretation, we collected additional Mössbauer spectra at 40 K and 30 K, which showed a gradual decline in the collapsed sextet and the appearance of defined sextets with temperature (SI 14). Therefore, we can compare the proportion of the collapsed sextet within the spectrum of the different samples as a measure of relative crystallinity of the samples. A greater proportion of a collapsed sextet implies higher crystallinity as ordering of the doublets into sextets has begun at a higher temperature relative to a sample with a lower proportion of a collapsed sextet. In the spectra collected here, the proportion of the collapsed sextet in the phosphate-free samples increased with pH, ranging from ~64% at pH 3 to ~93% at pH 6 and 8. At pH 3 and pH 6, in the presence of 1 mmol g^{-1} phosphate, this area reduced to 35% and 59%. Thus, the schwertmannite samples showed an increase in crystallinity with pH, and a decrease in crystallinity after reaction with phosphate.

4. Discussion

4.1. Effects of pH on sulfate release and the schwertmannite structure

In this study, we examined phosphate sorption at various, but constant pH. A buffered electrolyte solution and a 24-h pre-equilibration period was used to maintain a stable pH during phosphate sorption experiments despite the acidification caused by the replacement of hydroxide ions for schwertmannite's sulfate. In the following, we discuss the impacts of pre-equilibration of schwertmannite at variable pH, which resulted in sulfate release and subtle structural alterations.

4.1.1. Sulfate release during pre-equilibration at various pH

Depending on pH, up to 60% of the initially present sulfate in schwertmannite was released during the 24-h pre-equilibration period (Fig. 2), consistent with earlier studies (Jönsson et al., 2005). The release of sulfate thus far has primarily been attributed to the transformation to goethite (Bigham et al., 1996; Murad and Rojík, 2003; Regenspurg et al., 2004; Paikaray and Peiffer, 2010). However, the uncatalyzed transformation of schwertmannite to goethite takes much longer (>2 weeks) at room temperature than the here applied 24-h pre-equilibration period. Also, our XRD analyses did not indicate any signs of goethite formation (Fig. SI 3) nor did the SEM analyses show any changes in morphology (Fig. 5). Short-term sulfate release was therefore attributed to the replacement of sulfate groups by hydroxyl groups

through a ligand-exchange reaction. Hydroxyl groups replaced sulfate in a stable 2:1 ratio, independent of pH, thereby preserving schwertmannite's charge neutrality. Previous X-ray absorption spectroscopy (XAS) analyses identified the inner-sphere sulfate groups in schwertmannite as bidentate-binuclear bridging groups (Wang et al., 2015), presumably originating from the initial coordination environment of Fe^{3+} as dissolved Fe-SO$_4$ complexes in the acidic, sulfate-rich waters prior to nucleation of schwertmannite (Hawthorne et al., 2000). Assuming these groups are replaced by two Fe-OH groups (Parfitt and Smart, 1978), the ligand exchange for inner-sphere sulfate can be described by Eq. (5). The reaction also explains the base-neutralizing capacity of schwertmannite:

$$(5)$$
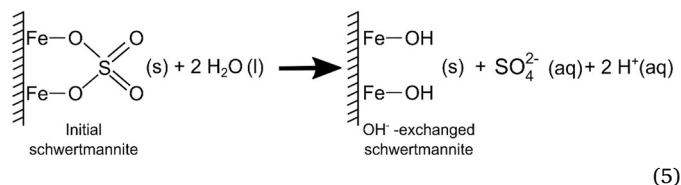
At alkaline pH, the concentration of H$^+$-ions decreases, causing the equilibrium of reaction Eq. (5) to shift towards sulfate release. After 24 h of pre-equilibration, 1.2 mmol SO$_4^{2-}$ g^{-1} was already released at pH 8 (equivalent to 52% of the initial sulfate), which decreased to 0.7 and 0.2 mmol SO$_4^{2-}$ g^{-1} for pH 6 and 3, respectively (Fig. 2a). Surface-bound sulfate ions are expected to be preferentially released (Jönsson et al., 2005). It has been previously proposed, based on extractions with nitrate, that sulfate in schwertmannite exceeding a molar S:Fe ratio of 1:8 is surface-bound sulfate (Bigham et al., 1990). In our study, this would indicate that 42% of the total sulfate resided on the surface, corresponding to 0.8 mmol SO$_4^{2-}$ g^{-1}. This is in line with earlier determinations of surface-sulfate, which amounted to 35–50% of all sulfate in the mineral phase (Bigham et al., 1990; Rose and Ghazi, 1997; Paikaray and Peiffer, 2010). We therefore conclude that at pH 3 and 6, where sulfate release was below 0.8 mmol SO$_4^{2-}$ g^{-1}, predominantly surface-sulfate, and less tunnel sulfate, was liberated. In contrast, at pH 8, (at least) an additional 0.4 mmol SO$_4^{2-}$ g^{-1} of tunnel sulfate must have been released to attain the equilibrium sulfate release of 1.2 mmol SO$_4^{2-}$ g^{-1}. The existence of two different sulfate pools at alkaline pH align with the fact that a two-step model was required to accurately describe sulfate release kinetics at pH 8. In contrast, at pH 3 and 6, a one-step pseudo-first order model was sufficient to represent sulfate release, suggesting sulfate release from similar exchange pools (Fig. 2a, SI 6).

4.1.2. Impact of pH on the structure and sulfate coordination of schwertmannite

Although a substantial amount of tunnel sulfate was released at pH 8, XRD showed no alterations in mineralogy (Fig. SI 4), nor did SEM reveal any changes in morphology (Fig. 5). Analysis by FTIR and Mössbauer spectroscopy, however, indicated nuanced modifications in the schwertmannite structure after equilibration at a more alkaline pH. Specifically, FTIR showed that at pH 8 (and to a lesser extent at pH 6), a larger proportion of the non-releasable sulfate was outer-spherically coordinated compared to pH 3. Although FTIR could not quantify this portion, previous XAS studies determined that 50% of total sulfate in schwertmannite was outer-sphere coordinated at pH 3, which increased to 90% and 100% at pH 6 and pH 8 (Wang et al., 2015). The 24 h-pre-equilibration at neutral to alkaline pH therefore had a two-fold effect on sulfate: (i) a replacement of sulfate by hydroxyl groups, thus increasing the amount of hydroxyl surface groups on schwertmannite, and (ii) the remaining sulfate in schwertmannite was predominantly present as outer-spherical complexes.

Equilibration at different pH also induced changes in the local environment around the Fe(III) atoms in the structure of schwertmannite (Cashion and Murad, 2012), which was assessed by ^{57}Fe Mössbauer spectroscopy. The ^{57}Fe Mössbauer spectra of the pH equilibrated schwertmannite samples were best fit with a combination of one or two doublets in addition to a partially ordered sextet (Fig. 8, Table 3). The presence of multiple components to fit the spectra indicates a diverse molecular environment around the Fe(III) atoms. This aligns with the observation that Fe(III) atoms in schwertmannite are surrounded by a combination of inner- and outer-sphere sulfate groups, along with hydroxyl groups (Cashion and Murad, 2012), resulting in the formation of distinct Fe(III) domains, each exhibiting their own Mössbauer signatures. Another explanation for the presence of multiple subspectra lies in the poorly constrained composition of schwertmannite, where more crystalline nanodomains are associated with a short-range order matrix, which is characterized by less structural arrangement or site defects. While this interpretation aligns with the suggested polycrystalline nature of schwertmannite (French et al., 2012), Mössbauer spectroscopy cannot conclusively identify the physical origin of the distinct Fe(III) sites. It is likely that different molecular environments around the Fe(III) atoms are the result of a combination of coordination and multiphase effects.

At pH 6 and 8, where the majority of sulfate groups was either outer-spherically coordinated or had been released (>50%), a significant proportion (>90%) of the Mössbauer spectra was fitted with a collapsed sextet, implying enhanced crystallinity compared to the pH 3 sample. A higher crystallinity with a lower concentration of inner-spherically bound sulfate can be understood by examining the molecular-scale structure of schwertmannite. Schwertmannite consists of double chains of Fe(III)-O octahedra that share corners, creating square tunnel cavities held together by sulfate (Schoepfer and Burton, 2021). When the inner-spherical bond between sulfate and the Fe—O framework breaks, a process that is favored at alkaline pH, the tunnel structure is no longer stabilized by sulfate and may collapse. This creates a structurally distorted schwertmannite which may serve as the precursor of goethite (Wang et al., 2015), where the squared octahedral channel in schwertmannite would lose two additional Fe(III)-O octahedra to transform into the rectangular arrangement of goethite (Fernandez-Martinez et al., 2010). The changes in the local environment of Fe caused by the replacement of $FeSO_4^-$ by Fe—O domains as identified by Mössbauer spectroscopy, did not lead to observable changes in long-range structural order (which would be detectable by XRD) nor visible morphological alterations (which are observable by SEM). Similar to previous findings for ferrihydrite (Latta et al., 2023), a more magnetically ordered phased initially formed, which was distinct from schwertmannite, but which did not yet results in a new mineral phase. This structural transition can be interpreted as a proto-transformation, potentially representing a crucial first step in the crystallization process of schwertmannite. This concept is consistent with the fact that schwertmannite is metastable with respect to goethite, especially under alkaline conditions (Wang et al., 2015).

Overall, our results demonstrate that the equilibration pH had substantial impacts on schwertmannite's affinity for sulfate. At a more alkaline pH, the mineral's surface increasingly consisted of hydroxyl groups, and schwertmannite's sulfate groups exhibited a higher degree of outer-sphere coordination. These changes not only affected the molecular structure of schwertmannite, but also had implications for its sorption properties regarding phosphate.

4.2. Impact of pH on schwertmannite's ligand exchange reaction

4.2.1. Relationship between sulfate affinity and phosphate sorption

Phosphate sorption reached a maximum of 1.7 mmol PO_4^{3-} g^{-1}, consistent with previous studies (0.65–2.8 mmol PO_4^{3-} g^{-1}) (Khamphila et al., 2017; Schoepfer et al., 2017; Bai et al., 2021; Fan et al., 2023). Notably, the highest sorption in this study occurred at pH 6, while the cited research only examined acidic pH conditions. This finding also distinguishes schwertmannite from non-sulfate-containing Fe(III) (oxy) hydroxides, which typically exhibit maximum phosphate sorption at acidic pH (Luengo et al., 2006; Huang et al., 2009). Generally, acidic pH allows for a higher surface site density of negatively-charged oxyanions because the surface groups on Fe(III) (oxy)hydroxides become increasingly protonated. Studies on the point-of-zero charge (PZC) have shown that schwertmannite's PZC is near-neutral (between 5.4 and 7.4), similar to iron oxides (Regenspurg, 2002). Hence, a difference in surface charge cannot explain the observed pH-effect on phosphate sorption. Interestingly, specific acid mine drainage soils, much like the schwertmannite studied here, also exhibited maximum phosphate sorption at a pH of 5.5 (Boukemara et al., 2017). Also, for arsenite, maximum sorption to schwertmannite occurred at pH 9 rather than at acidic pH (Burton et al., 2009). This suggests that the sorption maximum of oxyanions to schwertmannite is not dictated by surface charge alone.

The sorption maximum of 1.7 mmol PO_4^{3-} g^{-1} also exceeds what would be expected based on the specific surface area (SSA). The schwertmannite synthesized in our study had an SSA of 24 m^2 g^{-1}, which lies within the typical range for schwertmannite produced using this method (16 m^2 g^{-1}, Liu et al., 2015). However, this value appears relatively low compared to other studies of schwertmannite, which reported SSAs up to 220 m^2 g^{-1} (Bigham et al., 1990; Regenspurg et al., 2004). This discrepancy suggests that BET measurements may not fully capture the SSA of schwertmannite, possibly reflecting only the external surface area instead of the total SSA. Based on a typical surface site density of 3 μmol PO_4^{3-} m^{-2} for Fe(III) (oxy)hydroxides (Huang et al., 2009), the anticipated sorption maximum would be 0.072 mmol PO_4^{3-} g^{-1} (if a SSA of 24 m^2 g^{-1} is assumed), and 0.660 mmol PO_4^{3-} g^{-1} (if a SSA of 220 m^2 g^{-1} is assumed). Both values are much lower than the here observed 1.7 mmol PO_4^{3-} g^{-1}. This discrepancy provides further evidence that sorption to schwertmannite is not solely a surface process, but relies on exchange reactions involving sulfate- and hydroxyl groups.

The thermodynamic driving force for this exchange depends on the relative affinity of schwertmannite for phosphate compared to its affinity for sulfate groups (which form inner- and outer-spherical complexes in schwertmannite, depending on pH). Unfortunately, in the literature, no well-defined stability constants for sulfate groups of schwertmannite could be found. Also, because the structure of schwertmannite is complex and possibly polyphasic (French et al., 2012), stability constants of differently coordinated and located sulfate groups may vary within the mineral. Even though these are not necessarily specific to schwertmannite, commonly used stability constants in the literature are derived from those for Fe(III) (oxy)hydroxides (Paikaray and Peiffer, 2010; Schoepfer and Burton, 2021).

To gain a deeper insight into the phosphate sorption behaviour of schwertmannite, we conducted modeling of the ligand exchange reaction in PHREEQC (SI 15), utilizing the constants for Fe(III) (oxy)

hydroxides. In the pH-range 4.5 to 7, the amount of sorbed sulfate decreased, whereas the amount of sorbed phosphate remained unchanged. The decrease in sorbed sulfate marks sulfate's sorption edge. For pH levels exceeding 7, also phosphate sorption decreased strongly. Based on these thermodynamic calculations, the ligand exchange of phosphate for sulfate would therefore be most favourable in the pH range of 4.5–7, which aligns with the pH range where the sorption maximum was observed in our experiments (Fig. 3a).

The influence of pH on sulfate affinity is also reflected by our experimental results. At pH 3 and a phosphate loading of 1.5 mmol PO_4^{3-} g^{-1}, 60% of the sulfate remained within the mineral structure (Fig. 3b). These non-releasable sulfate groups can be regarded as inaccessible sorption sites in our pH 3 experiments. Conversely, at pH 6, only 9% of sulfate remained in the structure and a higher loading of 1.7 mmol PO_4^{3-} g^{-1} was achieved. Hence, the lower affinity of schwertmannite's sulfate groups at pH 6 meant that phosphate could more effectively exchange. At a more alkaline pH, the surface charge becomes more negative, which offsets the favourable effects that arise from the diminished affinity for sulfate. Possibly, also structural alterations (see Section 4.1.2) during pre-equilibration contributed to the lower phosphate sorption at pH 8. As a consequence, the sorption maximum was the lowest among the tested pH conditions (1.2 mmol PO_4^{3-} g^{-1}).

The observed effects of pH on surface charge, sulfate stability and phosphate sorption were further elucidated by quantifying the amount of sulfate and phosphate associated with the schwertmannite structure (Fig. 9). At pH 3 and high phosphate levels, a total of 2.3 mmol of oxyanions per gram were bound, but only 65% of them were phosphate ions. At pH 6, only 1.9 mmol of oxyanions were bound per gram, but 90% of these were phosphate. This proportion decreased to 1.7 mmol g^{-1}, with 75% being phosphate, at pH 8. Hence, sorption on schwertmannite involved a competitive exchange between schwertmannite's sulfate groups and the sorbing oxyanion. The pH-dependent sorption behaviour therefore differs from non-sulfate containing Fe(III) (oxy) hydroxides, where sulfate affinity does not play a role.

It should be noted that also the protonation of phosphate (pKa_1 = 2.1, pKa_2 = 7.2, pKa_3 = 12.7) and the type of phosphate surface complex that forms could have contributed to the observed pH-behaviour. Both bidentate or monodentate phosphate complexes can form on iron oxides (Arai and Sparks, 2001; Elzinga and Sparks, 2007), which undergo increased deprotonation at pH > 7.5. At more acidic pH, an increased proportion of sorbed phosphate is present as monodentate complexes
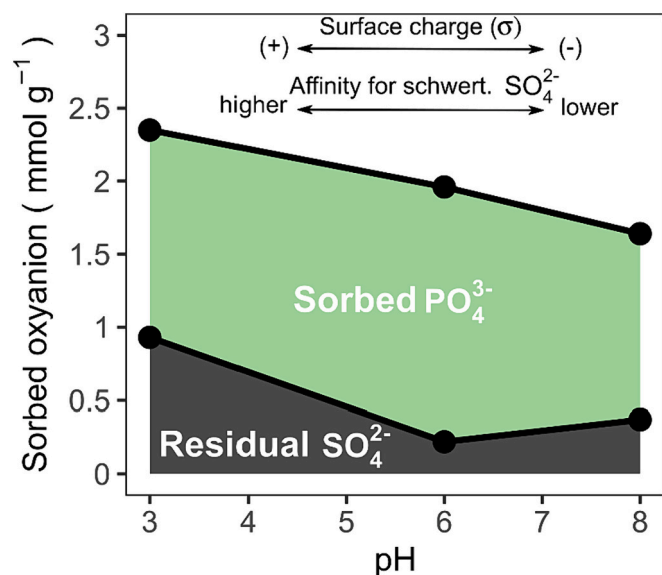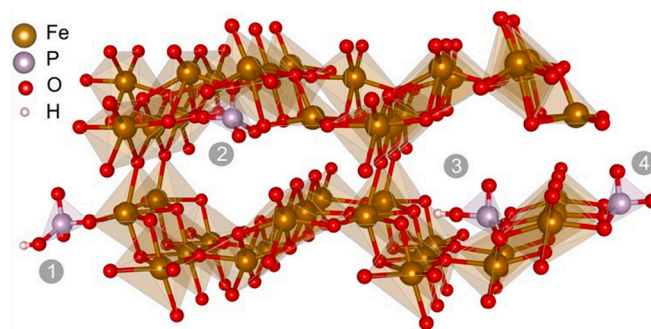

Fig. 10. Schematic Illustration of potential inner-sphere phosphate complexes on schwertmannite, as characterized by Arai and Sparks (2001) and Elzinga and Sparks (2007), including: (1) a protonated, monodentate complex; (2) a deprotonated, monodentate complex, (3) a protonated, bidentate complex; (4) a deprotonated, bidentate complex.
Phosphate complexes occur both in tunnel cavities and on the surface of schwertmannite. The schwertmannite structure (resolved by Fernandez-Martinez et al., 2010) was downloaded from the American Mineralogist Crystal Structure and visualized in VESTA (Momma and Izumi, 2011).

(Elzinga and Sparks, 2007). Exchange of a bidentate sulfate complex for a monodentate phosphate complex could also have contributed to the observed lower ligand exchange ratio (released sulfate:sorbed phosphate) under more acidic conditions. Fig. 10 illustrates a potential model of phosphate complexation on schwertmannite. Determination of the exact coordination complex of phosphate on schwertmannite still requires further research by more advanced spectroscopic techniques.

4.2.2. Effect of pH on the coordination of surface groups and sorption kinetics

In environmental sciences, a profound understanding of kinetics is essential as it enables us to assess the timeframes of diverse processes (Oldham et al., 2013). In this study, phosphate sorption to schwertmannite was satisfactorily described using a two-step kinetic model, which included a fast, nearly instantaneous, surface sorption process and a slower second process. Both processes were influenced by pH. Under more alkaline conditions, a higher amount of phosphate was sorbed in the fast step (Table 1). The initial sorption rate was one-and-a-half times faster at pH 6 compared to pH 3. In contrast, phosphate sorption to non-sulfate containing Fe(III) (oxyhydr)oxides is six times faster at pH 3 compared to pH 8 (Luengo et al., 2007; Stumm and Morgan, 2012). To understand the slower sorption rates at acidic pH for schwertmannite, we need to consider the effects of pH on sorption sites and sulfate affinity.

Previously, the fast process was attributed to exchange for surface-bound sulfates, while the slower step involved intraparticle diffusion of sorbing oxyanions and subsequent exchange for structurally bound sulfate (Marouane et al., 2021). Our results from the sorption experiments and findings from Wang et al. (2015), however, suggest five distinct sorption mechanisms for phosphate on schwertmannite, being exchange for: (i) hydroxyl groups, (ii) outer-sphere surface sulfate groups, (iii) inner-sphere surface sulfate groups, (iv) inner-sphere structural (tunnel) sulfate groups, and (v) outer-sphere structural (tunnel) sulfate groups. Fast-exchanging groups likely include lower-affinity outer-sphere surface sulfate groups and the surface hydroxyl groups. Slower sites may involve high-affinity, inner-sphere coordinated sulfate on the surface and inner- and outer-sphere sulfate groups in the tunnels. The pre-equilibration at more alkaline pH before phosphate addition led to the replacement of sulfate in schwertmannite by hydroxyl ions, resulting in the formation of surface hydroxyl groups. At pH 6 and 8, 90% to 100% of the residual sulfate groups became outer-sphere coordinated (Wang et al., 2015). Thus, at pH 6 and 8, a notably higher number of fast-exchange sites would have become accessible after the pre-equilibration step at the start of the sorption experiment. This led to

Fig. 9. Oxyanions bound to schwertmannite at the end of the sorption experiment for the high-phosphate treatment at pH 3, 6, and 8.

a 1.5- times increased initial sorption rate. Also, the decrease in the ratio of released sulfate to sorbed phosphate with increasing pH was a result of the sulfate having been replaced by hydroxyl ions during the 24-h equilibration-period.

The second slow sorption process on schwertmannite has previously been attributed to intraparticle diffusion (Dou et al., 2013; Marouane et al., 2021). However, also for the second step, the rate constant was found to be 20 times higher at pH 6 and 8 compared to pH 3. Similar observations were made for arsenate, where equilibration took longer at pH 4 than at pH 7 (Burton et al., 2009). This increase in the rate constant could be explained by tunnel sulfates also being present as more loosely bound outer-sphere groups at high pH, making them exchange more readily. Hence, the rate of the second process was controlled by a composite mechanism that included diffusion-based transport constraints and changes in sulfate affinity. The higher affinity of schwertmannite for phosphate also allows phosphate to sorb on sites that are inaccessible for sulfate (Tofan-Lazar and Al-Abadleh, 2012). This also explains the faster sorption rate of phosphate compared to sulfate release. In summary, the rate of the second process was controlled by a composite mechanism that included diffusion-based transport constraints and changes in sulfate affinity.

4.2.3. Impact of phosphate sorption on the structure of schwertmannite

Phosphate effectively replaced both tunnel and surface sulfates, while also exchanging for hydroxyl groups. Independent of pH, FTIR analysis (Fig. 7) showed vibration peaks resembling those observed for inner-sphere phosphate complexes on ferrihydrite and hematite (Arai and Sparks, 2001; Elzinga and Sparks, 2007). In analogy to these phosphate complexes, we therefore concluded that phosphate binds to schwertmannite by forming both bidentate-binuclear and monodentate complexes that undergo increased deprotonation at high pH. Effects of phosphate substitution on the long-range structure of schwertmannite, as indicated by XRD (Fig. SI 4), seemed minimal. Also, the typical sea-urchin morphology of schwertmannite remained unaltered (Fig. 5).

In contrast to these findings, ^{57}Mössbauer spectroscopy revealed clear changes in the immediate vicinity of the Fe(III)-atoms within the schwertmannite structure. Mössbauer spectra were fitted by a combination of a collapsed sextet and one or two doublet spectra. The proportion of the collapsed sextet was smaller in samples that had received phosphate compared to phosphate-free treatments (Fig. 8, Table 3). For phosphate-treated samples, the lower proportions of the collapsed sextet thus suggest an inhibition of the proto-transformation. It is likely that phosphate stabilized the low-crystalline schwertmannite structure against transformation to more crystalline phases by forming strong inner-spherical complexes, which then prevented a collapse of the Fe (III)-O tunnel framework. The stabilizing effect was also found for other oxyanions binding to schwertmannite (Shan et al., 2023). It is furthermore consistent with previous studies on phosphate binding to schwertmannite under reducing (i.e. Fe(II)- catalysed) conditions (Schoepfer et al., 2019).

A lower crystallinity compared to phosphate-free conditions also suggests an increased structural disorder resulting from phosphate-for-sulfate substitution. This is likely due to the smaller sulfate (ionic radius of 0.230 nm, Wilkinson and Gillard, 1987) being replaced by the larger phosphate ion (ionic radius of 0.238 nm). Replacement of sulfate with a larger oxyanion distorts the tunnel structure of schwertmannite, leading to a reduction in crystallinity (Regenspurg and Peiffer, 2005; Schoepfer et al., 2019). It is also plausible that structural defects are necessary to accommodate phosphate in the schwertmannite framework (Shan et al., 2023). Interestingly, this phenomenon was absent in the pH 8 samples, highlighting the need for further research. Spectroscopic methods like XAS could offer further insights into the mutual interactions between phosphate sorption and the structural transformation of schwertmannite.

5. Conclusions and implications

This study integrates phosphate sorption experiments across varied pH conditions with analyses of sulfate affinity to schwertmannite and changes in the mineral structure. We found that pH had a profound impact on both maximum phosphate sorption capacity and kinetics. Unlike sulfate-free Fe(III) (oxyhydr)oxides, phosphate sorption was highest at circumneutral pH, which we explained by the effects of pH on schwertmannite's affinity for sulfate. Increased pH leads to outer-sphere sulfate coordination and more available sorption sites. Faster phosphate sorption and sulfate release kinetics were observed in circumneutral conditions.

An intriguing aspect of our study is the occurrence of a more magnetically-ordered collapsed sextet, indicating the replacement of FeSO$_4$-sites with Fe-O-sites, especially during the equilibration of schwertmannite at high pH. This was interpreted as a proto-transformation of schwertmannite's structure as an initial step in the transformation towards a more crystalline mineral phase. It should be noted that although this structural change was fast (i.e. within days), schwertmannite continued to be the dominant mineral even after four weeks of equilibration at pH 8, as confirmed by XRD (SI 12). The emerging phase, even though temporary, may therefore represent an important but overlooked phase in environments where schwertmannite is abundant.

Our research has several practical implications for the use of schwertmannite as a sorbent in environmental remediation and in managing nutrient availability in cultivated acid sulfate soils. Importantly, our experiments demonstrated that schwertmannite exhibits a high phosphate sorption capacity at both low and near-neutral pH levels. This characteristic property underscores schwertmannite's relevance as a phosphate sorbent in acid sulfate soils, including cultivated ones where schwertmannite and elevated phosphate concentrations may coexist (Fitzpatrick et al., 2017a). In such environments, liming is a widespread practice that typically raises the pH of the topsoil to near-neutral levels (Sarangi et al., 2022).

Schwertmannite has also recently gained attention as a promising sorbent for wastewater treatment and for mitigating phosphate pollution in eutrophic surface waters with near-neutral pH (Simon and Burghard, 2016). Furthermore, it has been proposed as a low-cost and innovative sorbent for use in filter beds, particularly in agricultural landscapes (Janneck et al., 2015; Marouane et al., 2021). An advantage of using schwertmannite in these applications is its long-term persistence in the environment in the presence of high phosphate concentrations. However, while schwertmannite exhibits remarkable phosphate sorption capabilities, the results of this study also underpin the need to consider the potential negative effects on water quality of sulfate release caused by ligand exchange.

Our study highlights the need for further research on the interplay between structural changes and sorption properties, especially in the early stages of schwertmannite transformation. Based on our findings, we suggest that future research places a greater emphasis on investigating sulfate affinity for schwertmannite. An integrated approach, involving simultaneous investigation of oxyanion sorption, sulfate release, and structural studies, is essential for a thorough understanding of how pH influences schwertmannite's sorption properties.

CRediT authorship contribution statement

Karel As: Conceptualization, Data curation, Investigation, Formal Analysis, Methodology, Visualization, Writing – original draft. **Stefan Peiffer:** Conceptualization, Funding acquisition, Supervision, Writing – review & editing. **Peter Onyisi Uhuegbue:** Investigation, Methodology. **Prachi Joshi:** Investigation, Formal Analysis, Writing – review & editing. **Andreas Kappler:** Writing – review & editing. **Bouchra Marouane:** Conceptualization. **Kerstin Hockmann:** Conceptualization, Investigation, Formal Analysis, Methodology, Supervision, Writing – review &

editing.

Declaration of competing interest

The authors declare that they have no known competing financial interests or personal relationships that could have appeared to influence the work reported in this paper.

Data availability

Research Data associated with this article can be accessed at https://doi.org/10.5281/zenodo.10302801.

Acknowledgements

Appendix A. Supplementary data

Supplementary data to this article can be found online at https://doi.org/10.1016/j.chemgeo.2024.122043.

References

Antelo, J., Fiol, S., Gondar, D., López, R., Arce, F., 2012. Comparison of arsenate, chromate and molybdate binding on schwertmannite: Surface adsorption vs anion-exchange. J. Colloid Interface Sci. 386, 338–343. https://doi.org/10.1016/j.jcis.2012.07.008.
Appelo, C.A.J., Postma, D., 2013. PHREEQC (Version 3.0) [Computer software]. US Geological Survey. https://www.usgs.gov/software/phreeqc-version-3.
Arai, Y., Sparks, D.L., 2001. ATR-FTIR spectroscopic investigation on phosphate adsorption mechanisms at the ferrihydrite-water interface. J. Colloid Interface Sci. 241, 317–326. https://doi.org/10.1006/jcis.2001.7773.
Bai, S., Lü, W., Chen, S., Han, J., Liu, Z., Giwa, A.S., 2021. Different adsorption behavior of inorganic and organic phosphorus on synthetic schwertmannite: Assessment and mechanism of coexistence. J. Environ. Chem. Eng. 9, 106056 https://doi.org/10.1016/j.jece.2021.106056.
Baty, F., Ritz, C., Charles, S., Brutsche, M., Flandrois, J.-P., Delignette-Muller, M.-L., 2015. A toolbox for nonlinear regression in R: the package nlstools. J. Stat. Softw. 66, 1–21. https://doi.org/10.18637/jss.v066.i05.
Bigham, J.M., Schwertmann, U., Carlson, L., Murad, E., 1990. A poorly crystallized oxyhydroxysulfate of iron formed by bacterial oxidation of fe(II) in acid mine waters. Geochim. Cosmochim. Acta 54, 2743–2758. https://doi.org/10.1016/0016-7037(90)90009-A.
Bigham, J.M., Carlson, L., Murad, E., 1994. Schwertmannite, a new iron oxyhydroxysulfate from pyhäsalmi, Finland, and other localities. Mineral. Mag. 58, 641–648. https://doi.org/10.1180/minmag.1994.058.393.14.
Bigham, J.M., Schwertmann, U., Traina, S.J., Winland, R.L., Wolf, M., 1996. Schwertmannite and the chemical modeling of iron in acid sulfate waters. Geochim. Cosmochim. Acta 60, 2111–2121. https://doi.org/10.1016/0016-7037(96)00091-9.
Boily, J.-F., Gassman, P.L., Peretyazhko, T., Szanyi, J., Zachara, J.M., 2010. FTIR spectral components of schwertmannite. Environ. Sci. Technol. 44, 1185–1190. https://doi.org/10.1021/es902803u.
Boukemara, L., Boukhalfa, C., Azzouz, S., Reinert, L., Duclaux, L., Amrane, A., Szymczyk, A., 2017. Characterization of phosphorus interaction with sediments affected by acid mine drainage - relation with the sediment composition. Int. J. Sedim. Res. 32, 481–486. https://doi.org/10.1016/j.ijsrc.2017.09.004.
Brunauer, S., Emmett, P.H., Teller, E., 1938. Adsorption of gases in multimolecular layers. J. Am. Chem. Soc. 60 (2), 309–319. https://doi.org/10.1021/ja01269a023.
Burton, E.D., Bush, R.T., Johnston, S.G., Watling, K.Y.M.M., Hocking, R.K., Sullivan, L.A., Parker, G.K., 2009. Sorption of arsenic (V) and arsenic (III) to schwertmannite. Environ. Sci. Technol. 43, 9202–9207. https://doi.org/10.1021/es902461x.
Burton, E.D., Karimian, N., Johnston, S.G., Schoepfer, V.A., Choppala, G., Lamb, D., 2021. Arsenic-imposed effects on schwertmannite and jarosite formation in acid mine drainage and coupled impacts on arsenic mobility. ACS Earth Space Chem. 5, 1418–1435. https://doi.org/10.1021/acsearthspacechem.1c00047.

Byrne, J.M., Kappler, A., 2022. A revised analysis of ferrihydrite at liquid helium temperature using Mössbauer spectroscopy. Am. Mineral. 107 (8), 1643–1651. https://doi.org/10.2138/am-2021-7802.
Cashion, J.D., Murad, E., 2012. Mössbauer Spectra of the Acid Mine Drainage Mineral Schwertmannite from the Sokolov Basin, Czech Republic. Australia: N. P., 2012. Web.
Coates, J., 2006. Interpretation of Infrared Spectra, A Practical Approach Encyclopedia of Analytical Chemistry. John Wiley & Sons, Ltd.
Cornell, P.M., Schwertmann, U., 1996. The iron Oxides: Structure, Properties, Reactions, Occurrence and Uses. VCH Publishers, New York (570 p).
Dou, X., Mohan, D., Pittman, C.U., 2013. Arsenate adsorption on three types of granular schwertmannite. Water Res. 47, 2938–2948. https://doi.org/10.1016/j.watres.2013.01.035.
Elzinga, E.J., Sparks, D.L., 2007. Phosphate adsorption onto hematite: an in-situ ATR-FTIR investigation of the effects of pH and loading level on the mode of phosphate surface complexation. J. Colloid Interface Sci. 308, 53–70. https://doi.org/10.1016/j.jcis.2006.12.061.
Eneroth, E., Bender, Koch C., 2004. Fe-hydroxysulfates from bacterial Fe2+ oxidation. Hyperfine Interact. 156-157 (1–4), 423–429. https://doi.org/10.1023/B:HYPE.0000043263.25269.2f.
Eskandarpour, A., Sassa, K., Bando, Y., Okido, M., Asai, S., 2006. Magnetic removal of phosphate from wastewater using schwertmannite. Mater. Trans. 47, 1832–1837. https://doi.org/10.2320/matertrans.47.1832.
Fan, C., Guo, C., Chen, W., Tao, L., Yao, Q., Lu, G., Shen, Y., 2023. Colloids and surfaces A: physicochemical and engineering aspects chromate and phosphate adsorption on schwertmannite: competition, mobilization and mechanisms. Colloids Surf. A Physicochem. Eng. Asp. 658, 130691 https://doi.org/10.1016/j.colsurfa.2022.130691.
Fernandez-Martinez, A., Timon, V., Roman-Ross, G., Cuello, G., Daniels, J.E., Ayora, C., 2010. The structure of schwertmannite, a nanocrystalline iron oxyhydroxysulfate. Am. Mineral. 95, 1312–1322. https://doi.org/10.2138/am.2010.3446.
Fitzpatrick, R.W., Mosley, L.M., Raven, M.D., Shand, P., 2017a. Schwertmannite formation and properties in acidic drain environments following exposure and oxidation of acid sulfate soils in irrigation areas during extreme drought. Geoderma 308, 235–251. https://doi.org/10.1016/j.geoderma.2017.08.012.
Fitzpatrick, R.W., Shand, P., Mosley, L.M., 2017b. Acid sulfate soil evolution models and pedogenic pathways during drought and reflooding cycles in irrigated areas and adjacent natural wetlands. Geoderma 308, 270–290. https://doi.org/10.1016/j.geoderma.2017.08.016.
French, R.A., Caraballo, M.A., Kim, B., Rimstidt, J.D., Murayama, M., Hochella, M.F., 2012. The enigmatic iron oxyhydroxysulfate nanomineral schwertmannite: Morphology, structure, and composition. Am. Mineral. 97, 1469–1482.
Fukushi, K., Sato, T., Yanase, N., Minato, J., Yamada, H., 2004. Arsenate sorption on schwertmannite. Am. Mineral. 89, 1728–1734. https://doi.org/10.2138/am-2004-11-1219.
Gražulis, S., Daškevič, A., Merkys, A., Chateigner, D., Lutterotti, L., Quirós, M., Serebryanaya, N.R., Moeck, P., Downs, R.T., Le Bail, A., 2011. Crystallography Open Database (COD): an open-access collection of crystal structures and platform for world-wide collaboration. Nucleic Acids Res. 40, D420–D427. https://doi.org/10.1093/nar/gkr900. Jan.
Hawthorne, Frank, Krivovichev, Sergey, Burns, Peter, 2000. In: Alpers, C.N., Jambor, J. L., Nordstrom, D.K. (Eds.), The Crystal Chemistry of Sulfate Minerals p. 1-112 in Sulfate Minerals. Reviews in Mineralogy and Geochemistry, 40. Mineralogical Society of America.
Huang, X., Foster, G.D., Honeychuck, R.V., Schreifels, J.A., 2009. The maximum of phosphate adsorption at pH 4.0: why it appears on aluminum oxides but not on iron oxides. Langmuir 25, 4450–4461. https://doi.org/10.1021/la803302m.
Janneck, E., Burghardt, D., Simon, E., Peiffer, S., Paul, M., Koch, T., April 2015. Development of an adsorbent comprising schwertmannite and its utilization in mine water treatment. In: Proceedings of the International Mine Water Association, Santiago de Chile, Chile, pp. 21–24.
Jönsson, J., Persson, P., Sjöberg, S., Lövgren, L., 2005. Schwertmannite precipitated from acid mine drainage: phase transformation, sulfate release and surface properties. Appl. Geochem. 20, 179–191. https://doi.org/10.1016/j.apgeochem.2004.04.008.
Khamphila, K., Kodama, R., Sato, T., Otake, T., 2017. Adsorption and post adsorption behavior of schwertmannite with various oxyanions. J. Miner. Mater. Charact. Eng. 05, 90–106. https://doi.org/10.4236/jmmce.2017.52008.
Kraal, P., van Genuchten, C.M., Lenstra, W.K., Behrends, T., 2020. Coprecipitation of phosphate and silicate affects environmental iron (oxyhydr)oxide transformations: a gel-based diffusive sampler approach. Environ. Sci. Technol. 54, 12795–12802. https://doi.org/10.1021/acs.est.0c02352.
Knorr, K., Blodau, C., 2007. Controls on schwertmannite transformation rates and products. Appl. Geochem. 22, 2006–2015. https://doi.org/10.1016/j.apgeochem.2007.04.017.
Kraal, P., van Genuchten, C.M., Behrends, T., 2022. Phosphate coprecipitation affects reactivity of iron (oxyhydr)oxides towards dissolved iron and sulfide. Geochim. Cosmochim. Acta 321, 311–328. https://doi.org/10.1016/j.gca.2021.12.032.
Lagarec, K., Rancourt, D.G., 1997. Extended voigt-based analytic lineshape method for determining n-dimensional correlated hyperfine parameter distributions in Mössbauer spectroscopy. Nucl. Instrum. Methods Phys. Res., Sect. B 129, 266–280. https://doi.org/10.1016/S0168-583X(97)00284-X.
Latta, D., Rosso, K.M., Scherer, M.M., 2023. Tracking initial fe(II)-driven ferrihydrite transformations: a Mössbauer spectroscopy and isotope investigation. ACS Earth Space Chem. 7, 1814–1824. https://doi.org/10.1021/acsearthspacechem.2c00291.

Li, Y., Guo, H., Gao, Z., Ke, T., Zhu, Z., Cao, Y., Su, X., Wu, X., 2023. Phosphorus in shallow and deep groundwater: Importance of p/fe ratio in fe(III) oxides in aquifer sediments. J. Hydrol. 623, 129860 https://doi.org/10.1016/j.jhydrol.2023.129860.

Liu, F., Zhou, J., Zhang, S., Liu, L., Zhou, L., Fan, W., 2015. Schwertmannite synthesis through ferrous ion chemical oxidation under different H2O2 supply rates and its removal efficiency for arsenic from contaminated groundwater. PLoS One 10, 1–14. https://doi.org/10.1371/journal.pone.0138891.

Luengo, C., Brigante, M., Antelo, J., Avena, M., 2006. Kinetics of phosphate adsorption on goethite: comparing batch adsorption and ATR-IR measurements. J. Colloid Interface Sci. 300, 511–518. https://doi.org/10.1016/j.jcis.2006.04.015.

Luengo, C., Brigante, M., Avena, M., 2007. Adsorption kinetics of phosphate and arsenate on goethite. A comparative study. J. Colloid Interface Sci. 311, 354–360. https://doi.org/10.1016/j.jcis.2007.03.027.

Marouane, B., Klug, M., As, K.S., Engel, J., Reichel, S., Janneck, E., Peiffer, S., 2021. The potential of granulated schwertmannite adsorbents to remove oxyanions (SeO32−, SeO42−, MoO42−, PO43−, Sb(OH)6−) from contaminated water. J. Geochem. Explor. 223, 106708 https://doi.org/10.1016/j.gexplo.2020.106708.

Momma, K., Izumi, F., 2011. VESTA3 for three-dimensional visualization of crystal, volumetric and morphology data. J. Appl. Crystallogr. 44, 1272–1276. https://doi.org/10.1107/S0021889811038970.

Murad, E., Rojík, P., 2003. Iron-rich precipitates in a mine drainage environment: Influence of pH on mineralogy. Am. Mineral. 88 https://doi.org/10.2138/am-2003-11-1234.

Murphy, J., Riley, J.P., 1958. A single-solution method for the determination of soluble phosphate in sea water. J. Mar. Biol. Assoc. U. K. 37, 9–14. https://doi.org/10.1017/S0025315400014776.

Oldham, C.E., Farrow, D.E., Peiffer, S., 2013. A generalized damköhler number for classifying material processing in hydrological systems. Hydrol. Earth Syst. Sci. 17, 1133–1148. https://doi.org/10.5194/hess-17-1133-2013.

Paikaray, S., Peiffer, S., 2010. Dissolution kinetics of sulfate from schwertmannite under variable pH conditions. Mine Water Environ. 29, 263–269. https://doi.org/10.1007/s10230-010-0118-0.

Paikaray, S., Göttlicher, J., Peiffer, S., 2011. Removal of as(III) from acidic waters using schwertmannite: surface speciation and effect of synthesis pathway. Chem. Geol. 283, 134–142. https://doi.org/10.1016/j.chemgeo.2010.08.011.

Parfitt, R., Smart, R., 1978. The mechanism of sulfate adsorption on iron oxides1. Soil Sci. Soc. Am. J. 42 https://doi.org/10.2136/sssaj1978.03615995004200010011x.

Regenspurg, S., 2002. Characterisation of Schwertmannite : Geochemical Interactions with Arsenate and Chromate and Significance in Sediments of Lignite Opencast Lakes. PhD Thesis,. University Bayreuth. https://epub.uni-bayreuth.de/id/eprint/1010.

Regenspurg, S., Peiffer, S., 2005. Arsenate and chromate incorporation in schwertmannite. Appl. Geochem. 20, 1226–1239. https://doi.org/10.1016/j.apgeochem.2004.12.002.

Regenspurg, S., Brand, A., Peiffer, S., 2004. Formation and stability of schwertmannite in acidic mining lakes. Geochim. Cosmochim. Acta 68, 1185–1197.

Rose, S., Ghazi, A.M., 1997. Release of sorbed sulfate from iron oxyhydroxides precipitated from acid mine drainage associated with coal mining. Environ. Sci. Technol. 31, 2136–2140.

Rouquerol, J., Rouquerol, F., Llewellyn, P., Maurin, G., Sing, K., 2013. Adsorption by Powders and Porous Solids: Principles, Methodology and Applications. Academic press.

Sarangi, S.K., Mainuddin, M., Maji, B., 2022. Problems, management, and prospects of acid sulfate soils in the ganges delta. Soil Syst. 6 https://doi.org/10.3390/soilsystems6040095.

Schoepfer, V.A., Burton, E.D., 2021. Schwertmannite: a review of its occurrence, formation, structure, stability and interactions with oxyanions. Earth Sci. Rev. 221, 103811 (doi: j.earscirev.2021.103811).

Schoepfer, V.A., Burton, E.D., Johnston, S.G., Kraal, P., 2017. Phosphate-imposed constraints on schwertmannite stability under reducing conditions. Environ. Sci. Technol. 51, 9739–9746. https://doi.org/10.1021/acs.est.7b02103.

Schoepfer, V.A., Burton, E.D., Johnston, S.G., 2019. Contrasting effects of phosphate on the rapid transformation of schwertmannite to fe(III) (oxy)hydroxides at near-neutral pH. Geoderma 340, 115–123. https://doi.org/10.1016/j.geoderma.2018.12.051.

Shan, J., He, M., Liu, P., Wang, W., Lin, C., Ouyang, W., Liu, X., Zhou, J., Xie, H., 2023. Antimony immobilization mechanism on schwertmannite: Insights from the microstructure of schwertmannite. Geochim. Cosmochim. Acta 359, 71–83. https://doi.org/10.1016/j.gca.2023.09.005.

Simon, D.A.R., Burghard, Elisabeth A.N.D., 2016. Removal of oxoanions from water: Comparison of a novel schwertmannite adsorbent and an iron hydroxide adsorbent. In: Proceedings IMWA 2016, Freiberg/Germany.

Stumm, W., Morgan, J.J., 2012. Aquatic Chemistry: Chemical Equilibria and Rates in Natural Waters. John Wiley & Sons.

Tabatabai, M.A., 1974. A rapid method for determination of sulfate in water samples. Environ. Lett. 7, 237–243. https://doi.org/10.1080/00139307409437403.

Tofan-Lazar, J., Al-Abadleh, H.A., 2012. Kinetic ATR-FTIR studies on phosphate adsorption on iron (oxyhydr)oxides in the absence and presence of surface arsenic: Molecular-level insights into the ligand exchange mechanism. Chem. Eur. J. 116, 10143–10149. https://doi.org/10.1021/jp308913j.

Wang, X., Gu, C., Feng, X., Zhu, M., 2015. Sulfate local coordination environment in schwertmannite. Environ. Sci. Technol. 49, 10440–10448. https://doi.org/10.1021/acs.est.5b02660.

Wang, X., Wang, Z., Peak, D., Tang, Y., Feng, X., Zhu, M., 2018. Quantification of coexisting inner- and outer-sphere complexation of sulfate on hematite surfaces. ACS Earth Space Chem. 2 https://doi.org/10.1021/acsearthspacechem.7b00154.

Wang, X., Ying, H., Zhao, W., Feng, X., Tan, W., Beyer, K.A., Huang, Q., Liu, F., Zhu, M., 2021. Molecular-scale understanding of sulfate exchange from schwertmannite by chromate versus arsenate. Environ. Sci. Technol. 55, 5857–5867. https://doi.org/10.1021/acs.est.0c07980.

Weng, Y., Vekeman, J., Zhang, H., Chou, L., Elskens, M., Tielens, F., 2020. Unravelling phosphate adsorption on hydrous ferric oxide surfaces at the molecular level. Chemosphere 261, 127776. https://doi.org/10.1016/j.chemosphere.2020.127776.

Wilkinson, G., Gillard, R.D., 1987. Comprehensive Coordination Chemistry the Synthesis, Reactions, Properties and Applications of Coordination Compounds. Main Group and Early Transition Elements. Pergamon Press, United Kingdom (ISBN: 0–08–026232-5 (7 v)).

Winland, R.L., Traina, S.J., Bigham, J.M., 1991. Chemical composition of ochreous precipitates from Ohio coal mine drainage. J. Environ. Qual. 20, 452–460. https://doi.org/10.2134/jeq1991.00472425002000020019x.

Yu, Q., Kandegedara, A., Xu, Y., Rorabacher, D.B., 1997. Avoiding interferences from good's buffers: a contiguous series of noncomplexing tertiary amine buffers covering the entire range of pH 3–11. Anal. Biochem. 253, 50–56. https://doi.org/10.1006/abio.1997.2349.